| | |
|---|---|
| Title | Wireless ferroelectric resonating sensor |
| Author(s) | Viikari, Ville; Seppä, Heikki; Mattila, Tomi; Alastalo, Ari |
| Citation | IEEE Transactions on Ultrasonics, Ferroelectrics, and Frequency Control vol. 57(2010):4, pp. 785-791 |
| Date | 2010 |
| URL | http://dx.doi.org/10.1109/TUFFC.2010.1482 |
| Rights | Copyright © [2010] IEEE. Reprinted from IEEE Transactions on Ultrasonics, Ferroelectrics, and Frequency Control vol. 57(2010):4, pp. 785-791. |

# Wireless Ferroelectric Resonating Sensor

Ville Viikari, *Member, IEEE*, Heikki Seppä, Tomi Mattila, and Ari Alastalo

***Abstract*—This paper presents a passive wireless resonating sensor that is based on a ferroelectric varactor. The sensor replies with its data at an intermodulation frequency when a reader device illuminates it at 2 closely located frequencies. The paper derives a theoretical equation for the response of such a sensor, verifies the theory by simulations, and demonstrates a temperature sensor based on a ferroelectric varactor.**

## I. Introduction

Wireless sensors are passive, battery-assisted semi-passive, or active that contain a radio transmitter and a battery. The advantages of passive sensors are that their lifetime or operation conditions are not limited by the battery and that they are inexpensive. Examples of passive wireless sensors are silicon-based radio frequency identification (RFID) tags, surface acoustic wave (SAW) RFID, and inductively coupled resonance-circuit sensors.

The RFID tags are based on integrated circuits (ICs), which enable several sophisticated features such as rewritable memory and anticollision protocols. The cost of an RFID tag is low due to its high manufacturing volumes. RFID is mostly used for identification but can also be used to realize other sensors by adding a sensing element to the tag [1], [2]. Passive RFID has some disadvantages. The power rectifier that generates the required power for the IC limits the largest read-out distance and the highest operation frequency. Therefore, RFID is not well suited for applications where a long distance or a high operation frequency is required. High operation frequencies are needed to enable small tag sizes and accurate spatial localization of the tag.

SAW tags transform the electromagnetic energy to SAWs propagating on a piezoelectric substrate. The SAWs are then manipulated and transformed back to electromagnetic waves. The SAW tags lend themselves well as sensors because the propagation properties of SAWs can be tailored to be sensitive to several measured quantities, such as temperature or strain, and no external sensor element is necessarily needed, although it is possible to use one [3]. The SAW sensors are reviewed in [4]. The highest operation frequency is typically limited to a few gigahertz by the line width of acoustical reflectors fabricated on the substrate.

Inductively coupled resonance-circuit sensors are used, for example, to measure strain [5] and moisture [6]. These sensors consist of a simple electrical resonance circuit, whose resonance frequency is sensitive to the measured quantity. The simple sensor structure enables a low manufacturing cost. However, these sensors cannot be read across large distances, because they require near-field coupling to the reader device.

Passive wireless sensors can also be implemented with the microelectromechanical systems (MEMS) technology [7]. The MEMS sensor, when illuminated with two different frequencies, responds with the sensor data at an intermodulation frequency. The intermodulation interrogation concept [8] is somewhat similar to the harmonic radar that was first proposed for traffic applications [9] and later was used for tracking insects [10]–[12] and avalanche victims [13]. The advantage of the intermodulation over harmonic mixing is that the smaller frequency offset between the transmitted and received signals facilitates the circuit design and enables fulfillment of the frequency regulations.

The intermodulation radar is proposed for determining the presence of metal corrosion in reinforcing steel members in concrete structures [14] and for automotive radars to detect pedestrians, cyclists, and other road users who are at high risk of serious injury in a traffic accident [15]. A general radar concept using nonlinear properties of the radar target is presented in [16].

This paper presents a sensor that is based on a ferroelectric varactor and is interrogated using the intermodulation mixing principle. The sensor offers a simple architecture similar to the inductively coupled resonance-circuit sensors, but the interrogation distance can be significantly larger. The demonstrated sensor architecture is well suited for applications where a wired readout is difficult, for example, due to harsh operating conditions, rotating parts, or cost and complexity of wiring. An obvious potential application field is temperature measurements in industrial machinery and engines. The ferroelectric varactor can be cost effectively realized using thin-film manufacturing technologies and is a solid-state device, both of which can be advantageous, e.g., over the MEMS-based nonlinear elements. Ultimately, there exists promise for very low-cost mass production of the entire sensor using the printed electronics manufacturing methods [17], [18].

## II. Operation Principle of the Sensor

The sensor consists of a ferroelectric varactor that is conjugate matched to an antenna. The equivalent electrical circuit of the sensor is shown in Fig. 1. The antenna

Manuscript received July 20, 2009; accepted December 1, 2009. This work was supported in part by the EU Commission under the contract FP7-ICT-2007-1-216049 of the ADOSE project.

The authors are with VTT Technical Research Centre, Espoo, Finland (e-mail: ville.viikari@vtt.fi, heikki.seppa@vtt.fi, tomi.mattila@vtt.fi, ari.alastalo@vtt.fi).

Digital Object Identifier 10.1109/TUFFC.2010.1482

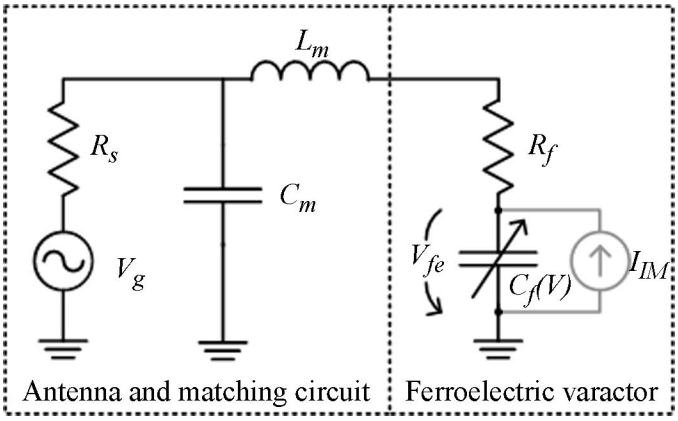


Fig. 1. The electrical equivalent circuit of the sensor based on a ferroelectric varactor.

is represented as an equivalent voltage source with the voltage $V_g$ and the internal resistance $R_s$. The matching circuit consists of the shunt capacitance $C_m$ and the series inductance $L_m$ and may either be included into the antenna or it may be realized as a separate circuit. The resistance $R_f$ represents the losses of the varactor and $C_f(V)$ relates the nonlinear capacitance to the voltage. The current source in parallel with the nonlinear capacitance is used to represent the modulated current over the varactor in the following analysis.

The presented sensor can be realized using any nonlinear element, but the following analysis considers a barium strontium titanate varactor $Ba_xSr_{1-x}TiO_3$ (BST) in paraelectric mode. This varactor has a symmetric $C$-$V$ curve at zero bias and lends itself well to produce intermodulation mixing products.

### *A. Intermodulation Response of the Sensor*

In what follows, an equation relating the actuation signals at two frequencies to the sensor response at an intermodulation frequency is derived. The same low actuation power level is assumed for the both input frequencies.

The sensor antenna is represented as an equivalent voltage source, as shown in Fig. 1, producing a voltage

$$V_g = 2\sqrt{2P_{\text{in}}R_s}\left(\cos\omega_1 t + \cos\omega_2 t\right), \tag{1}$$

where $P_{\text{in}}$ is the received power at one frequency, $R_s$ is the equivalent resistance of the antenna, and $\omega_1$ and $\omega_2$ are the angular frequencies of the actuation signals. The voltage over the varactor is approximately

$$\begin{aligned} V_{fe} &\approx \frac{2\sqrt{2P_{\text{in}}R_s}\left(\cos\omega_1 t + \cos\omega_2 t\right)}{j\omega C_{\max}\left(R_s + \left(Z_f + j\omega L_m\right)\left(1 + j\omega C_m R_s\right)\right)} \\ &= \hat{V}_{fe}\left(\cos\omega_1 t + \cos\omega_2 t\right), \end{aligned} \tag{2}$$

where $Z_f = R_f + 1/(j\omega C_{\max})$ is the impedance of the ferroelectric varactor, $R_f$ is the voltage-independent series resistance of the varactor, and $C_{\max}$ is the zero-voltage capacitance of the varactor. For simplicity, it is assumed that the electrical bandwidth of the system is much larger than the frequency difference between $\omega_1$ and $\omega_2$, i.e., $\omega \approx \omega_1 \approx \omega_2$.

The voltage dependence of a BST paraelectric varactor can be expressed as [19]

$$C_f(V) = \frac{C_{\max}}{2\cosh\left[\frac{2}{3}\sinh^{-1}\left(\frac{2V}{V_{1/2}}\right)\right] - 1}, \tag{3}$$

where $C_{\max}$ is the maximum capacitance and $V_{1/2}$ is the voltage at which the capacitance is halved. The capacitance can be approximated at small voltages with the second-order Taylor's expansion as

$$C_f(V) \approx C_{\max}\left(1 - \frac{16}{9}\frac{V^2}{V_{1/2}^2}\right). \tag{4}$$

The modulated current over the varactor is approximately

$$I_f = j\omega C_f(V_{fe})V_{fe} \approx j\omega C_{\max}V_{fe}\left(1 - \frac{16}{9}\frac{V_{fe}^2}{V_{1/2}^2}\right). \tag{5}$$

Substituting (2) into (5) gives the current component at an intermodulation frequency

$$\begin{aligned} I_{fe,\text{IM}} = -\frac{4}{3}&\left(\frac{2\sqrt{2P_{\text{in}}R_s}}{\left(R_s + \left(Z_f + j\omega L_m\right)\left(1 + j\omega C_m R_s\right)\right)}\right)^3 \\ &\times \cos\left(\left(2\omega_1 - \omega_2\right)t\right). \end{aligned} \tag{6}$$

This current is produced by the equivalent current source in parallel with the varactor, as shown in Fig. 1. The radiated power (equivalently the power dissipated in $R_s$) at an intermodulation frequency is

$$P_{\text{IM}} = \left(\frac{16\sqrt{2}R_s^2 P_{in}}{3V_{1/2}^2\omega^3 C_{\max}^3\left|R_s + \left(Z_f + j\omega L_m\right)\left(1 + j\omega C_m R_s\right)\right|^4}\right)^2 P_{\text{in}}. \tag{7}$$

### *B. Exploitation as a Sensor*

The presented concept allows the wireless measurement of two sensor parameters: the resonance frequency ($f_r$) and the quality factor ($Q$). The wireless sensor can be implemented by designing the sensor such that either $f_r$ or $Q$ or both are sensitive to the measured quantity, such as temperature, strain, or humidity. The presented ferroelectric device can be used as a temperature sensor. The capacitance of the ferroelectric varactor is typically a strong function of the temperature [20].

The effective impedance of an ideal paraelectric varactor is power independent at small power levels that were

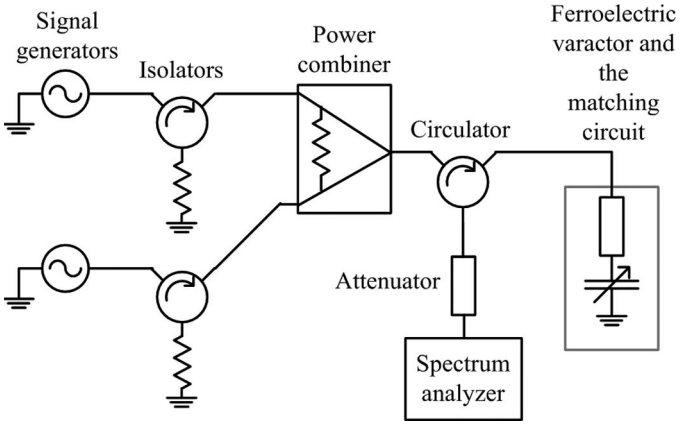


Fig. 2. The measurement setup for measuring the intermodulation conversion efficiency and the temperature of the ferroelectric device.

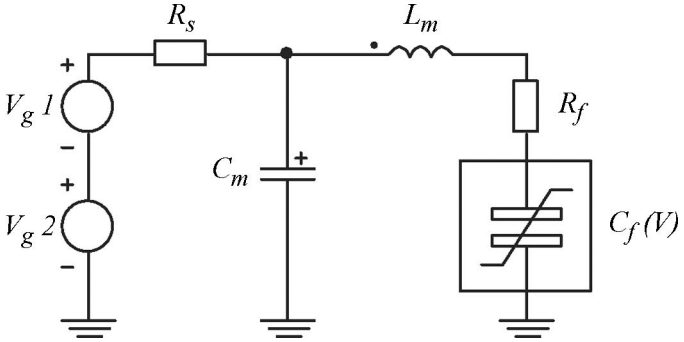


Fig. 3. The circuit schematic for simulating the intermodulation response of the ferroelectric varactor in APLAC. Earlier, similar models in APLAC were effectively used to model the complex nonlinear Duffing effect and intermodulation behavior in, for example, the microelectromechanical devices [21]–[23].

assumed above in the derivation of the intermodulation response of the varactor. When interrogating a sensor, the small signal assumption can be validated, for example, by comparing the sensor responses measured at different power levels.

## III. Experiments and Simulations

### A. Measurement Setup

The wired measurement setup that is used to measure the intermodulation frequency response of the sensor is shown in Fig. 2. The two input tones are generated with signal generators (Agilent E8257D and Agilent E8257C, Agilent Technologies, Inc., Palo Alto, CA) and fed through isolators, power combiner, and circulator to the tested device. The reflected signal is separated with the circulator and fed to a spectrum analyzer (FSEM, Rohde & Schwarz, Munich, Germany) that is used to measure the power at the intermodulation frequency. An attenuator is applied in front of the spectrum analyzer to suppress the third order mixing in the analyzer's mixer. The varactor is shorted at DC using a bias-T to avoid its possible self-biasing.

In the temperature sensor demonstration, the ferroelectric device is cooled down in a cryogenic probing station (BCT-21MRFZ, Nagase & Co. Ltd., Tokyo, Japan). For reference, the temperature dependence of the varactor's zero-voltage capacitance is measured with the impedance analyzer.

In addition to the wired measurement, the intermodulation response of the sensor is measured wirelessly. The circulator is connected to a broadband horn antenna (BBHA 9120 A, Schwarzbeck—Mess Elektronik, Schönau, Germany) and the ferroelectric sensor is connected to a half-wavelength dipole antenna with a coaxial cable. The half-wavelength antenna is placed outside the cryogenic probing station such that the distance between the antennas is 0.4 m.

### B. Simulations

The intermodulation response of the ferroelectric sensor was simulated with the Aplac software (AWR, El Segundo, CA, http://web.awrcorp.com/) using the harmonic balance simulation including harmonic frequencies up to third order. The circuit schematic of the ferroelectric sensor is shown in Fig. 3. The voltage dependent capacitance of the ferroelectric varactor is modeled with the dynamic voltage-controlled current source whose charge as a function of the voltage is given as

$$Q(V) = \frac{3C_{\max}V_{1/2}}{2}\sinh\left(\frac{1}{3}\sinh^{-1}\left(\frac{2V}{V_{1/2}}\right)\right). \tag{8}$$

The charge-voltage dependence given in (8) is the voltage-integral of (3) and is equivalent to the $C$-$V$ – curve given in (3) [19].

### C. Measured and Simulated Ferroelectric Sensor

The ferroelectric sensor consists of a ferroelectric varactor matched to $R_s = 50\ \Omega$ at 1.35 GHz with a series inductor and a shunt capacitor as shown in Fig. 1. The measured zero-voltage capacitance of the varactor at 290 K is $C_{\max} = 1.2$ pF with the series resistance of $R_f = 3.7\ \Omega$. The voltage at which the capacitance is halved was measured with an impedance analyzer (4294A, Agilent Technologies) at 110 MHz at different excitation voltages from 10 to 500 mV and was found to be $V_{1/2} = 7.5$ V independent of the applied excitation. The nominal values of the matching inductor and capacitors are 13 nH (±5%) (LQW04AN13NJ00, Murata Manufacturing Co., Kyoto, Japan) and 10.3 pF, respectively. Inductance value of 12.7 nH was used in the simulations and calculations, and it was found to provide the best fit. The inductance value providing the best fit is well within the tolerance limits given by the manufacturer. The parameters of the ferroelectric sensor that are used in the simulations and calculations are summarized in Table I.

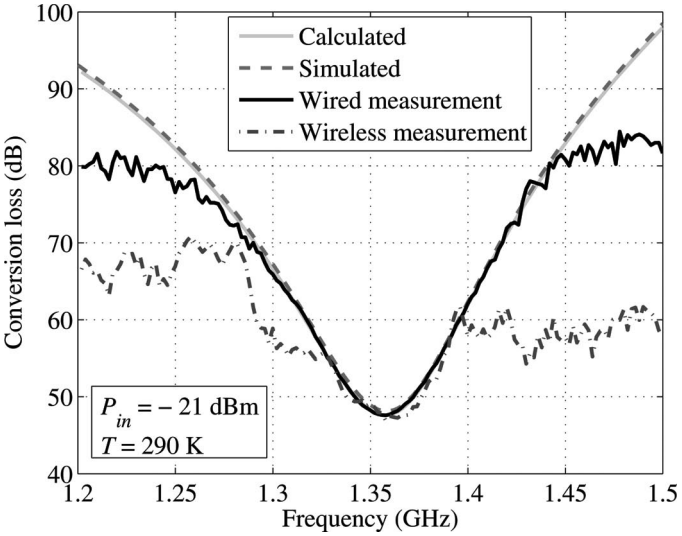


Fig. 4. The calculated, simulated, and measured conversion loss of the sensor as a function of the frequency. The absolute power level in the wirelessly measured curve may not be precise.

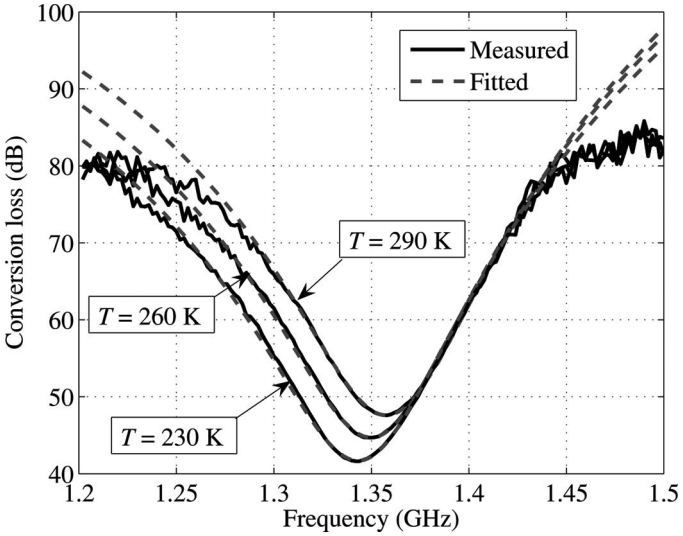


Fig. 5. The measured and fitted conversion losses as a function of the frequency. Different curves are for different temperatures.

TABLE I. The Parameters of the Ferroelectric Sensor Used in the Simulations and Calculations.

| | |
|---|---|
| Zero-voltage capacitance | $C_{\max} = 1.2$ pF |
| Series resistance of the varactor | $R_f = 3.7\ \Omega$ |
| Voltage at which the capacitance is halved | $V_{1/2} = 7.5$ V |
| Matching series inductance[1] | $L_m = 12.7$ nH |
| Matching shunt capacitance | $C_m = 10.3$ pF |

[1]Fitted to the measurements.

### D. Frequency Response of the Sensor

Fig. 4 shows the calculated, simulated, and measured intermodulation conversion losses ($P_{\text{in}}/P_{\text{IM}}$) of the sensor as a function of the frequency. The frequency offset between the signals is 100 kHz and the signal strength is −21 dBm. The sensor is at 290 K temperature. The absolute power level in the wireless measurement is not accurate, because the measurement was not performed in an anechoic chamber and antennas were not fully characterized.

The calculated, simulated, and measured conversion losses agree well. The minor deviations in the wirelessly measured curve are likely due to slight mismatch of the sensor antenna. Note that the low signal-to-noise–ratio in the wireless measurement prevents measurement of high conversion loss values.

### E. Temperature Response of the Sensor

The temperature affects both $V_{1/2}$ and $C_{\max}$ of the ferroelectric varactor. According to (7), $V_{1/2}$ has constant effect to the conversion loss at all frequencies, whereas $C_{\max}$ affects also the matching frequency. The prototype device is used as a temperature sensor by measuring the frequency response of the conversion loss and finding $C_{\max}$ that provides the best fit between the theoretical and measured responses defined as

$$\min_{A,C_{\max}} \left\{ \left( AL_{\text{meas}}(f) - L_{\text{calc}}(f, C_{\max}) \right)^2 \right\}, \tag{9}$$

where $L_{\text{meas}}$ is the measured frequency response of the conversion loss, $L_{\text{calc}}$ is the calculated frequency response of the conversion loss, and $A$ is the signal attenuation.

Fig. 5 shows the measured conversion loss of the sensor at 290, 260, and 230 K temperatures with the fitted curves.

The measured temperature response of the varactor's zero-voltage capacitance $C_{\max}$ is shown in Fig. 6. The temperature response is measured both using wired and wireless setups using the intermodulation principle. Also shown is the varactor capacitance directly measured using the impedance analyzer.

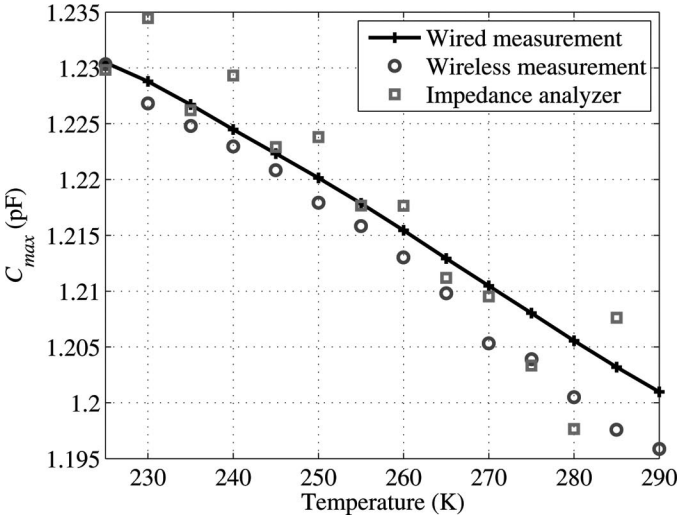


Fig. 6. The measured temperature responses of the sensor.

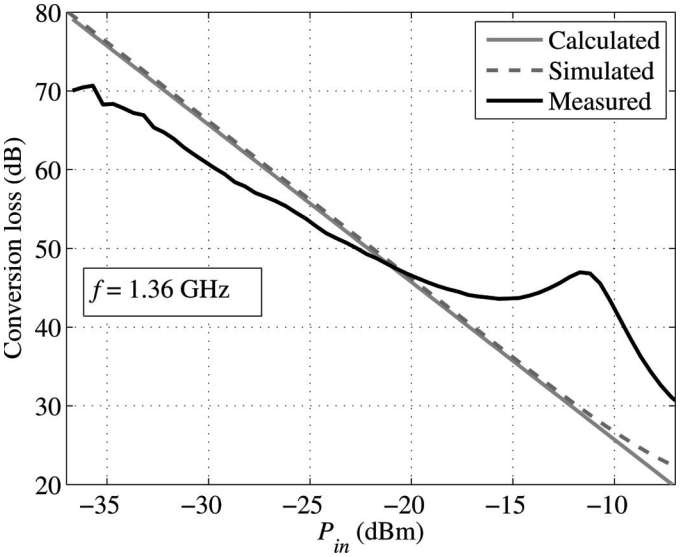


Fig. 7. The measured, calculated, and simulated conversion loss of the sensor at 1.36 GHz as a function of the input power level.

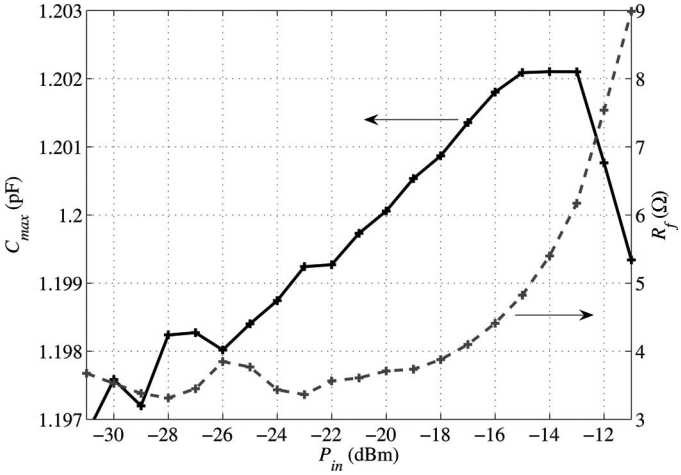


Fig. 8. The fitted parameters of the ferroelectric varactor at different power levels.

According to the measurement performed with wired connection, $C_{\max}$ changes linearly with the temperature. The results of the wireless measurement exhibit slight deviation from those of wired measurements. The deviations are due to lower signal-to-noise ratio and slight mismatch of the sensor antenna impedance, which is not taken into account in the fitting process. The capacitance value of the varactor is small for the impedance analyzer for precise measurement, and, therefore, the results obtained with the analyzer exhibit relatively large variations. However, the overall trend obtained with the impedance analyzer corresponds well to that measured with the intermodulation principle.

Note that the temperature resolution of the sensor could be increased by using ferroelectric material whose permittivity is more sensitive to the temperature.

### *F. Power Response of the Sensor*

The measured, simulated, and calculated conversion losses of the sensor as a function of the input power are shown in Fig. 7.

The slope of the measured conversion loss slightly differs from the calculated and simulated ideal response. The deviation is likely to be due to the power dependency of the impedance of the ferroelectric varactor. The simulated conversion loss verifies that the effect is not due to the change of the effective capacitance of the varactor, which takes place at much higher power levels ($\sim -5$ dBm, seen as the small deviation of the simulated response from the calculated one in the lower right corner). Instead, the varactor used is not perfectly ideal, and its impedance depends on the applied voltage. This could be because, for example, the varactor is not ideally paraelectric but also has parasitic ferroelectric (switchable, spontaneous polarization) properties.

The effect of the input power to the measurement accuracy of the sensor was further quantified by measuring the intermodulation frequency response of the sensor at $T = 290$ K at different power levels and finding $C_{\max}$ and $R_f$ giving the best fit between the measurements and calculations. The fitted values at different input power levels are shown in Fig. 8.

According to the fit in Fig. 8, both the resistance $R_f$ and the capacitance $C_{\max}$ of the ferroelectric varactor show a minor power dependency. The capacitance change in the used input power range from $-31$ to $-11$ dBm is 5 fF ($\sim 0.4\%$ relative change), which corresponds to approximately $\pm 5$-K uncertainty in the temperature measurement presented in Fig. 5. We emphasize that the power dependency is due to the unoptimized prototype character of the applied ferroelectric varactors and can be improved by further varactor development. The power dependency can also be mitigated, e.g., by performing the measurements at different power levels.

### *G. Detection Distance of the Sensor*

The detection distance of the sensor depends heavily on the intermodulation conversion efficiency of the sensor $P_{\mathrm{IM}}/P_{\mathrm{in}}$ given in (7). The highest conversion efficiency of the experimental sensor is limited by the input power at which the equivalent impedance of the ferroelectric varactor becomes power dependent. In the present case, the corresponding input power is approximately $-20$ dBm and the conversion loss 47 dB.

Assuming a 20-dBm transmit power, a 10-dBi reader antenna gain, a 3-dBi sensor antenna gain, and a receiver sensitivity of $-110$ dBm, the detection distance of the prototype sensor is 8 m at 1.35 GHz. The power received by the sensor at 8 m would be $-20$ dBm, at which the measured intermodulation conversion loss is 50 dB. The corresponding link budget calculation is presented in Table II.

The detection distance of the sensor depends heavily on the intermodulation conversion efficiency of the sensor

TABLE II. THE CALCULATED LINK BUDGET OF THE FERROELECTRIC SENSOR INTERROGATED WITH A READER DEVICE.

| | |
|---|---|
| Transmitted power | $P_t = 10$ dBm |
| Reader antenna gain | $G_{\text{reader}} = 10$ dBi |
| Free space loss | $\left(\frac{\lambda}{4\pi r}\right)^2 = -53$ dB |
| Sensor antenna gain | $G_{\text{sensor}} = 3$ dBi |
| Received power by the sensor | $P_{\text{sensor}} = -20$ dBm |
| Intermodulation mixing loss | $L = 47$ dB |
| Sensor antenna gain | $G_{\text{sensor}} = 3$ dBi |
| Free space loss | $\left(\frac{\lambda}{4\pi r}\right)^2 = -53$ dB |
| Reader antenna gain | $G_{\text{reader}} = 10$ dBi |
| Received power at intermodulation frequency | $P_r = -107$ dBm |

$P_{\text{IM}}/P_{\text{in}}$ given in (7). In principle, the conversion efficiency can be made very high by decreasing $V_{1/2}$ or by increasing the electrical quality factor of the sensor resonance. For example, the barium proportion of a BST varactor affects its $V_{1/2}$ [20]. The electrical quality factor of a ferroelectric varactor depends on the conductor and dielectric losses and ranges from 10 to several hundreds for thin-film varactors at gigahertz frequencies [24]. Consequently, the detection distance of the sensor could be even tens of meters at a few gigahertz frequencies.

## IV. CONCLUSION

This paper has presented a principle for a novel passive wireless sensor based on a ferroelectric varactor. The sensor is interrogated by illuminating it at two closely located frequencies and recording the backscattered signal at the intermodulation frequency. The paper has derived a theoretical equation for the intermodulation response of the sensor for low actuation power level. The analytical equation is verified by simulations and experiments. A passive wireless temperature sensor based on a ferroelectric varactor is demonstrated at 1.35 GHz.

## REFERENCES


[1] R. Want, "Enabling ubiquitous sensing with RFID," *Computer*, vol. 37, no. 4, pp. 84–86, Apr. 2004.

[2] A. P. Sample, D. J. Yeager, P. S. Powledge, A. V. Mamishev, and J. R. Smith, "Design of an RFID-based battery-free programmable sensing platform," *IEEE Trans. Instrum. Meas.*, vol. 57, no. 11, pp. 2608–2615, Nov. 2008.

[3] R. Steindl, A. Pohl, and F. Seifert, "Impedance loaded SAW sensors offer a wide range of measurement opportunities," *IEEE Trans. Microw. Theory Tech.*, vol. 47, no. 12, pp. 2625–2629, Dec. 1999.

[4] L. Reindl, G. Scholl, T. Ostertag, H. Scherr, U. Wolff, and F. Schmidt, "Theory and application of passive SAW radio transponders as sensors," *IEEE Trans. Ultrason. Ferroelectr. Freq. Control*, vol. 45, no. 5, pp. 1281–1292, Sep. 1998.

[5] J. C. Butler, A. J. Vigliotti, F. W. Verdi, and S. M. Walsh, "Wireless, passive, resonant-circuit, inductively coupled, inductive strain sensor," *Sens. Actuators A Phys.*, vol. 102, no. 1–2, pp. 61–66, Dec. 2002.

[6] J. Voutilainen, "Methods and instrumentation for measuring moisture in building structures," D.Sc. dissertation, Dept. Elect. Comm. Eng., Helsinki Univ. Technology, Espoo, Finland, 2005.

[7] V. Viikari and H. Seppä, "RFID MEMS sensor concept based on intermodulation distortion," *IEEE Sens. J.*, vol. 9, no. 12, pp. 1918–1923, Dec. 2009.

[8] D. E. N. Davies and R. J. Klensch, "Two-frequency secondary radar incorporating passive transponders," *IEE Electron. Lett.*, vol. 9, no. 25, pp. 592–593, Dec. 1973.

[9] H. Staras and J. Shefer, "Harmonic radar detecting and ranging system for automotive vehicles," US Patent 3781879, Dec. 25, 1973.

[10] E. T. Cant, A. D. Smith, D. R. Reynold, and J. L. Osborne, "Tracing butterfly flight paths across the landscape with harmonic radar," *Proc. Biol. Sci.*, vol. 272, no. 1565, pp. 785–790, Apr. 2005.

[11] J. R. Riley and A. D. Smith, "Design considerations for an harmonic radar to investigate the flight of insects at low altitude," in *Computers and Electronics in Agriculture*. Amsterdam, The Netherlands: Elsevier, 2002, vol. 35, pp. 151–169.

[12] B. G. Colpitts and G. Boiteau, "Harmonic radar transceiver design: Miniature tags for insect tracking," *IEEE Trans. Antenn. Propag.*, vol. 52, no. 11, pp. 2825–2832, Nov. 2004.

[13] Recco AB, Lidingö, Sweden. [Online]. Available: www.recco.com.

[14] H. Kwun, G. L. Burkhardt, and J. L. Fisher, "Detection of reinforcing steel corrosion in concrete structures using non-linear harmonic and intermodulation wave generation," US Patent 5 180 969, Jan 19, 1993.

[15] V. Viikari, J. Saebboe, S. Cheng, M. Kantanen, M. Al-Nuaimi, T. Varpula, A. Lamminen, P. Hallbjörner, A. Alastalo, T. Mattila, H. Seppä, P. Pursula, and A. Rydberg, "Technical solutions for automotive intermodulation radar for detecting vulnerable road users," in *Proc. IEEE 69th Vehicular Technology Conf.*, Barcelona, Spain, Apr. 26–29, 2009, pp. 1–5.

[16] A. Deutsch, A. Rosenberger, and I. Schnitzer, "Radar system and method for locating and identifying objects by their non-linear echo signals," European Patent EP 1 744 177, Jan 17, 2007.

[17] R. Åberg, "Printed non-volatile memory," in *Proc. Printed Electronics Asia 2008*, Tokyo, Japan, pp. 1–27.

[18] A. Alastalo, "PriMeBits EU FP7 Project on Printed Memories," in *Proc. Printed Electronics Europe 2009*, Dresden, Germany, Apr. 7–8, 2009, pp. 1–13.

[19] D. R. Chase, L.-Y. Chen, and R. A. York, "Modelling the capacitive nonlinearity in thin-film BST varactors," *IEEE Trans. Microw. Theory Tech.*, vol. 53, no. 10, pp. 3215–3220, Oct. 2005.

[20] A. K. Tagantsev, V. O. Sherman, K. F. Astafiev, J. Venkatesh, and N. Setter, "Ferroelectric materials for microwave tunable applications," *J. Electroceram.*, vol. 11, no. 1-2, pp. 5–66, 2003.

[21] T. Veijola and T. Mattila, "Modeling of nonlinear micromechanical resonators and their simulation with the harmonic-balance method," *Int. J. Microw. Millimet. Wave Comput. Aided Eng.*, vol. 11, no. 5, pp. 310–321, Aug. 2001.

[22] V. Kaajakari, T. Mattila, A. Oja, and H. Seppä, "Nonlinear limits for single-crystal silicon microresonators," *IEEE J. Microelectromech. Syst.*, vol. 13, no. 5, pp. 715–724, Oct. 2004.

[23] A. Alastalo and V. Kaajakari, "Third-order intermodulation in microelectromechanical filters coupled with capacitive transducers," *IEEE J. Microelectromech. Syst.*, vol. 15, no. 1, pp. 141–148, Feb. 2006.

[24] S. S. Gevorgian and E. L. Kollberg, "Do we really need ferroelectrics in paraelectric phase only in electrically controlled microwave devices?" *IEEE Trans. Microw. Theory Tech.*, vol. 49, no. 11, pp. 2117–2124, Nov. 2001.



**Ville V. Viikari** (S'06–A'09–M'09) was born in Espoo, Finland, in 1979. He received the M.S. (Tech.), Licentiate of Science (Tech.) (with distinction), and D.Sc. (Tech.) (with distinction) degrees in electrical engineering from the Helsinki University of Technology (TKK), Espoo, Finland, in 2004, 2006, and 2007, respectively.

From 2001 to 2007, he was a trainee, assistant researcher, and researcher with the Radio Laboratory, TKK, where he studied antenna measurement techniques at submillimeter wavelengths and antenna pattern correction techniques. He is currently a research scientist with the VTT Technical Research Centre in Espoo, Finland, and a docent with TKK. His current research interests are RFID systems and wireless sensors.

Dr. Viikari received the Young Scientist Award at URSI XXXI Finnish Convention on Radio Science, Espoo, Finland, October 28, 2008, and the best student paper award in the annual symposium of the Antenna Measurement Techniques Association, Newport, RI, October 30–November 4, 2005.

**Heikki Seppä** was born in Kortesjärvi, Finland, in 1953. He received the D.Sc. (Tech.) degree from the Helsinki University of Technology (TKK), Espoo, Finland, in 1989.

From 1976 to 1979 he was an assistant at TKK, where he studied low-temperature physics and electrical metrology. In 1979, he joined the Technical Research Centre, Espoo, Finland, mainly to develop the quantum metrology. In 1989, he was appointed a research professor at VTT. His research is focused on metrology, quantum devices, sensors, and especially on MEMS, wireless technology, and nanotechnology. He worked several months at NIST USA (1982–1983) developing ultra low-temperature noise thermometer and, in 2004, he was a tutoring professor in Nokia's Leading Science program.

**Tomi Mattila** (M'00) received M.S. (1994) and D.Sc. (Tech.) (1997) degrees from the Department of Technical Physics at Helsinki University of Technology, Espoo, Finland.

Since 1999, he has been working as senior research scientist at VTT Technical Research Center of Finland.

**Ari Alastalo** received the M.S. and D.Sc. (Tech.) degrees in technical physics from Helsinki University of Technology (TKK), Espoo, Finland, in 1997 and 2006, respectively. From 1996 to 1998, he was an assistant at TKK working in the area of magnetic quantum impurities. From 1998 to 2001, he was with Nokia Research Center carrying out research in radio propagation, RF architectures, baseband algorithms, and protocols for adaptive-antenna systems. Since 2002, he has been a research scientist at VTT focusing on microelectromechanical systems (MEMS), adaptive RF frontends, and printable electronics. Since 2006, he has led a research team at VTT focusing on inorganic printed electronics.